JTTEE5 2:329-338

Laser Processing of Plasma-Sprayed R-Ba-Cu-O Coatings

B. Arsenault, B. Champagne, D. Dubé, P. Lambert, and C. Gélinas

Thick Y-Ba-Cu-O and Er-Ba-Cu-O coatings were deposited by plasma spraying onto nickel substrates. These plasma-sprayed coatings were laser melted to modify their microstructures. The effects of primary processing conditions, such as linear energy and number of passes, on microstructural modifications were assessed. The microstructure of the as-sprayed coatings was largely transformed to produce a fine Y_2O_3 dispersion in a Ba-Cu-O matrix. A very low level of coating/substrate interactions can be maintained by appropriate laser processing conditions.

1. Introduction

PLASMA spraying is a deposition method that has the potential to produce large quantities of thick high-temperature superconductor (HTSC) coatings on parts with complex geometries that may be used for electrotechnical applications. To date, studies on plasma-sprayed HTSC coatings have shown that, due to the rapid solidification of the material during deposition, the loss of oxygen, and the noncongruent melting of $RBa_2Cu_3O_x$ compounds (R = rare earth), as-deposited coatings are not superconducting. Therefore, post-deposition treatments are required to restore superconductivity.[1-5] Furthermore, to obtain critical currents acceptable for practical applications, post-treatments must be carried out at high temperature in the partially molten state to promote alignment of large $RBa_2Cu_3O_x$ grains. Indeed, texturing treatments are well-established methods to overcome the weak link problem associated with the low critical currents in these HTSC materials.[6-10] However, in composite structures comprising a metallic component, diffusion of metal atoms into the superconducting phase is observed during these high-temperature post-treatments. This diffusion of metal atoms can largely reduce the critical transition temperature (T_c) of the superconducting phase and even destroy superconductivity.

Laser processing offers a means to modify the microstructure of plasma sprayed HTSC coatings by local remelting.[11,12] It is worth mentioning that the major advantage of laser processing over other types of melt processing techniques comes from the high thermal gradients generated by the laser in very small melt pools. Laser-melted layers can therefore be rapidly quenched by conduction into the substrate, refining microstructures and reducing the superconductor contamination by the substrate. Laser melting and quenching could be used for preparing a precursor coating consisting of very fine R_2O_3 phases well dispersed in a homogeneous and dense Ba-Cu-O matrix[13] for further texturing. These fine features increase reaction rates and improve completeness of the reaction for obtaining the superconducting 123 grains during texturing.

Key Words: fine microstructure, laser processing, phase analysis, RBaCuO coatings, superconductors

B. Arsenault, B. Champagne, D. Dubé, P. Lambert, and **C. Gélinas,** Industrial Materials Institute, National Research Council Canada, 75 De Mortagne Blvd., Boucherville, Québec, Canada, J4B 6Y4.

In this preliminary work, $YBa_2Cu_3O_x$ and $ErBa_2Cu_3O_x$ coatings were plasma sprayed onto nickel substrates and then laser processed to develop a new precursor coating. The objective of this investigation was to study the evolution of the microstructure induced in the coatings by laser processing.

2. Experimental Procedure

2.1 *Starting Materials*

Two series of specimens were prepared. Yttrium-base powders and erbium-base powders were used as starting materials for plasma spraying. A physical description of these powders is given in the next section. The first series of coatings was plasma sprayed using a 99.9% pure commercial Metco yttrium-base powder (spray dried and flame sprayed) with a stoichiometry corresponding to $YBa_2Cu_4O_8$ (Y-124). The excess of copper with respect to the 123 stoichiometry was suggested to compensate for the copper losses occurring during the deposition of particles.[1] The erbium-base powder with a stoichiometry corresponding to $ErBa_2Cu_3O_x$ (Er-123 where $6.5 < x < 7$) was prepared in the laboratory. As discussed later, no excess of copper was required because plasma spraying parameters were adjusted to reduce the vaporization of copper. The Er-123 powder was synthesized by solid-state reaction of $BaCO_3$, CuO, and Er_2O_3 using repeated sintering cycles in air at 930 °C with intermediate grinding and sieving to the size range of 10 to 64 μm.

2.2 *Substrate Preparation*

The substrate consisting of 0.75-mm thick nickel strips of 99.5% purity was degreased carefully and grit blasted with 24

Table 1 Process parameters for plasma spraying

	1st series: Y-base coatings	2nd series: Er-base coatings
Arc voltage, V	76	28
Arc current, A	450	350
Feed rate, g/min	28	32
Primary gas flow, L/min	70 (N_2)	48 (Ar)
Carrier gas flow, L/min	8.5 (O_2)	9 (Ar)
Stand off distance, cm	10	7.5
Coating thickness, μm	200	100

mesh alumina particles at a pressure of 500 kPa. They were then washed using acetone and rinsed with ethanol.

2.3 *Plasma Spraying*

Atmospheric plasma spraying was carried out with a Bay State plasma torch using the spray parameters listed in Table 1. The nickel substrates were not preheated during plasma spraying. For the Y-base coatings, relatively high energy plasma spray parameters were selected (34.2 kW). Nitrogen plasma gas was chosen to increase the enthalpy of the plasma and the particle dwell time in the plasma, thereby improving the melting of particles and increasing coating density. Coatings about 200 μm thick were built by depositing successive layers approximately

Table 2 Laser operating parameters

Parameter No.	Preheating temperature, °C	Scanning speed, mm/s	Incident power, W	Linear energy, J/mm
First series: Y-base coatings	20			
1		50	50	1.0
2		100	85	0.85
3		100	50	0.5
Second series: Er-base coatings	800			
4		500	100	0.2
5		1000	100	0.1
6		2000	115	0.06
7		4000	110	0.03

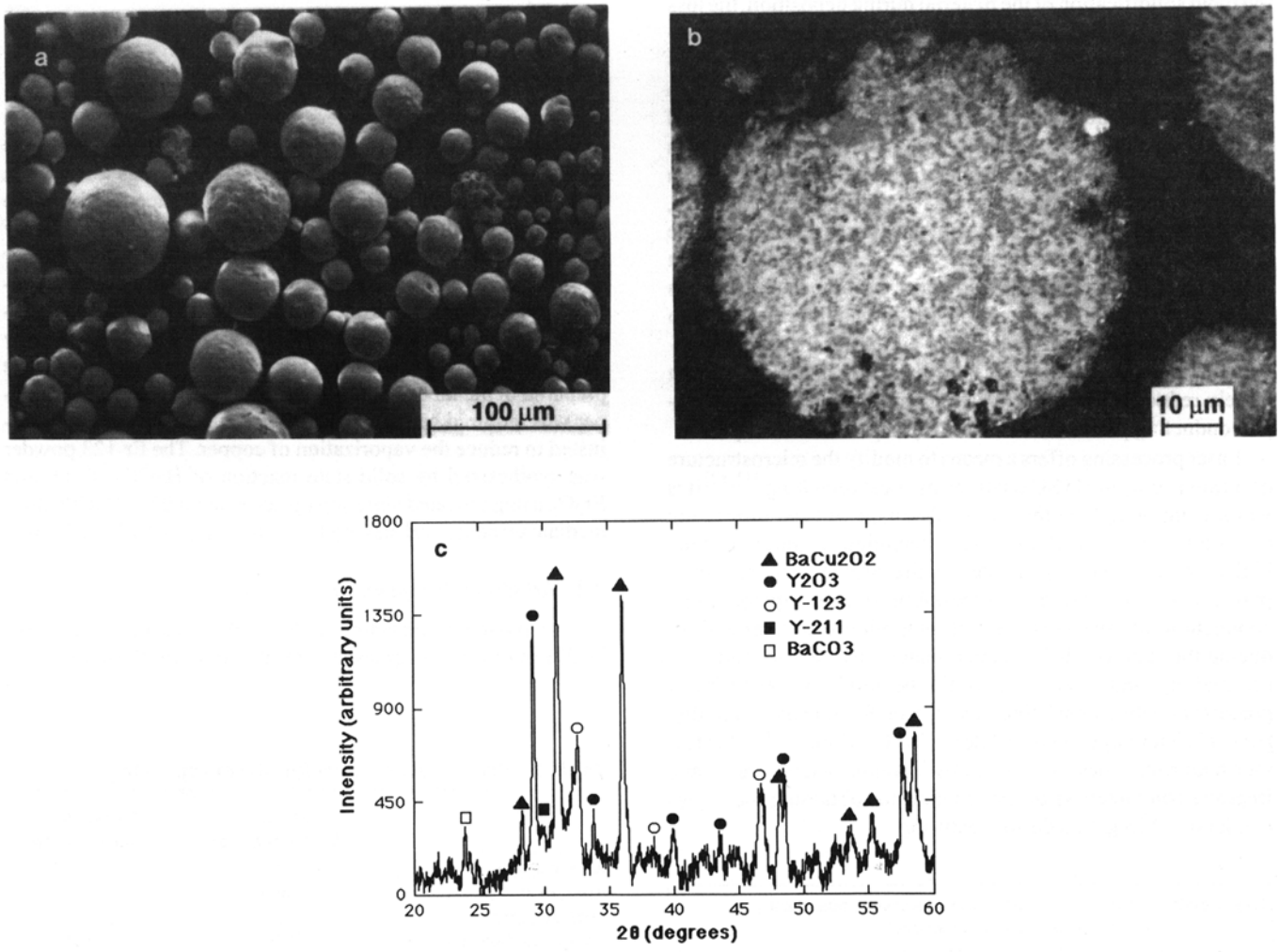

Fig. 1 Y-Ba-Cu-O powder used for plasma spraying. (a) Morphology of the starting powder. (b) Cross section of a particle. (c) XRD pattern of the powder.

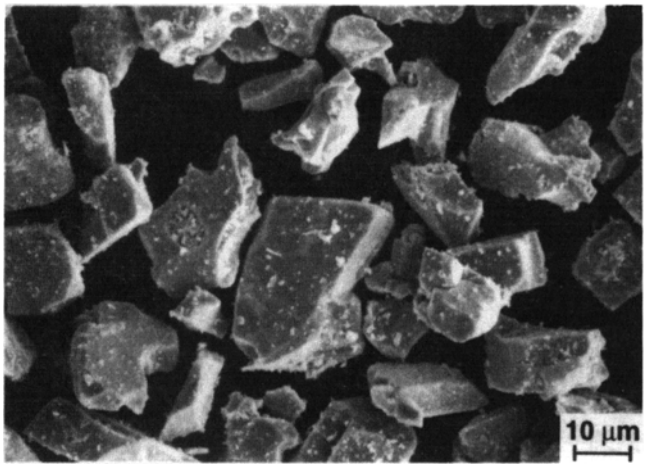

Fig. 2 Morphology of the Er-base powder used for plasma spraying.

30 to 40 μm thick. For the Er-base coatings, lower energy plasma spray parameters were selected (9.8 kW) to produce 100-μm thick coatings. After spraying, coatings were rapidly transported to vacuum storage to protect them from degradation by humidity and carbon dioxide.[14]

2.4 *Laser Processing*

Laser processing was performed using a 100-W CO_2 laser (MPB Technology LVPS-100) in continuous wave mode. The coatings were secured to a numerically controlled *X-Y* table under the laser beam, which was incident through Zn-Se optics. The incident laser beam was normal to the sample surface at focus yielding a 160-μm diameter beam. Oxygen flowed parallel to the laser beam onto the surface of specimens. The laser power was measured with a power meter (Coherent 2000 model). Surface coverage was achieved through a rectangular pattern with a

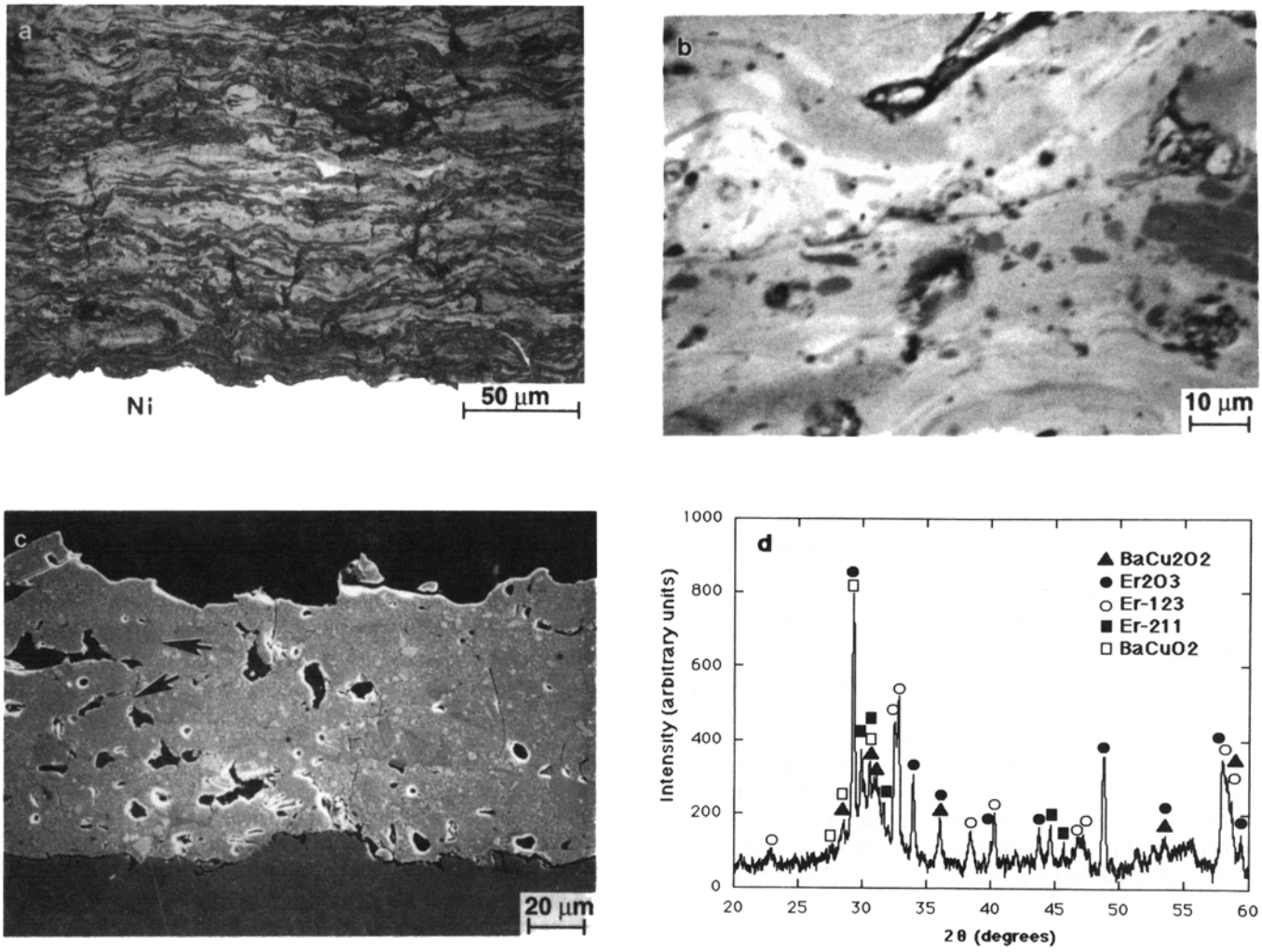

Fig. 3 As-deposited plasma-sprayed coatings. (a) Cross section of the Y-base coating. (b) High-magnification view of the Y-base coating showing lamellae and unevenly dispersed phases. (c) Cross section of the Er-base coating showing unmelted particles (see arrows) and porosities. (d) XRD pattern of the Er-base coating.

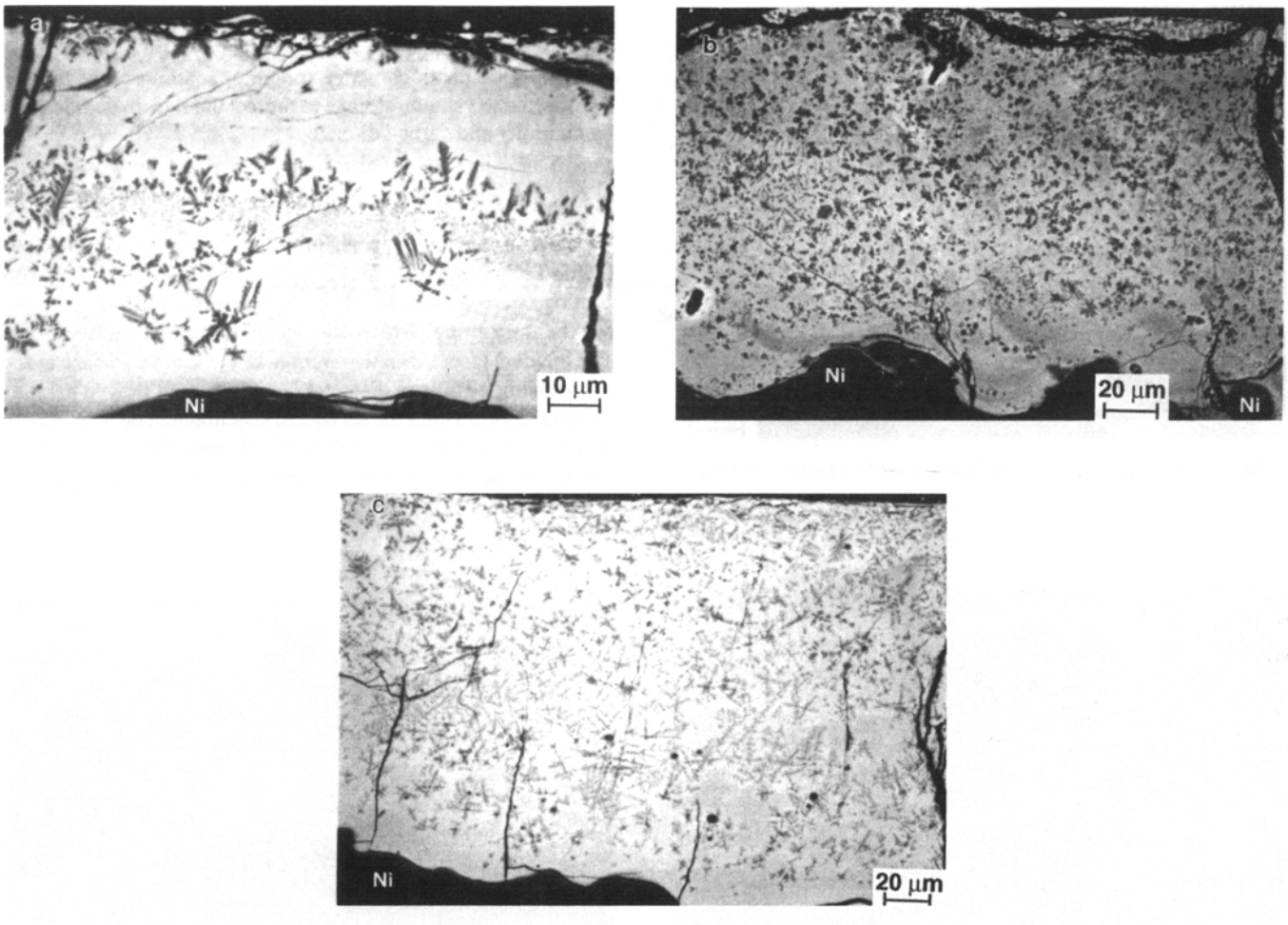

Fig. 4 Cross section of the Y-base coating after laser processing using (a) 1.0 J/mm, (b) 0.85 J/mm, and (c) 0.5 J/mm. These processing conditions are described as No. 1, 2, and 3, respectively, in Table 2.

translation of 100 μm between successive scans. Various laser parameters such as power density, sweep speed of specimens, and number of laser scans were studied. Seven different laser processing parameters (Table 2) were evaluated. The Y-base coatings were laser processed at room temperature, whereas the Er-base coatings were preheated on a hot stage at 800 °C during laser treatment. This preheating compensates for the lower incident energy input and helps reduce cracking.

Various operating conditions were investigated to assess the effect of primary process variables such as incident laser power and sweep velocity, which primarily control the laser/material interaction. For a given beam size, the extent of laser/material interaction can roughly be related to the linear energy, which is expressed as: $E_L = P/V_s$; where E_L is the linear energy (J/mm), P is the incident power (W), and V_s is the sweep velocity (mm/s). The effect of the linear energy was systematically varied from sample to sample (see Table 2). With the first series of coatings, the effect on the microstructure of three high linear energies was examined. Also, the effect of multiple scans was also investigated for one set of processing conditions. With the second series of coatings, the linear density of energy was further decreased.

The microstructure of coatings before and after laser processing was characterized by scanning electron microscopy (SEM), and the chemical composition of phases was assessed by X-ray dispersive spectroscopy (EDX). X-ray powder diffraction (XRD) using Cu K_α radiation was also performed on ground coatings extracted from nickel strips to determine the crystalline nature of the compounds in the coatings.

3. Results and Discussion

3.1 *Starting Materials*

The Y-base powder used in the first series of experiments is characterized in Fig. 1. Particles are mostly spherical (10 to 75 μm diameter) with a few sponge-like particles, which suggests that complete melting occurred during the fabrication of this powder by flame spraying (Fig. 1a). The powder cross section shown in Fig. 1(b) is a matrix containing finely dispersed precipitates. EDX analysis showed that the matrix is mostly the $BaCu_2O_2$ phase[15,16] instead of $BaCuO_2$, and the precipitates are Y_2O_3. The XRD pattern (Fig. 1c) confirmed the above re-

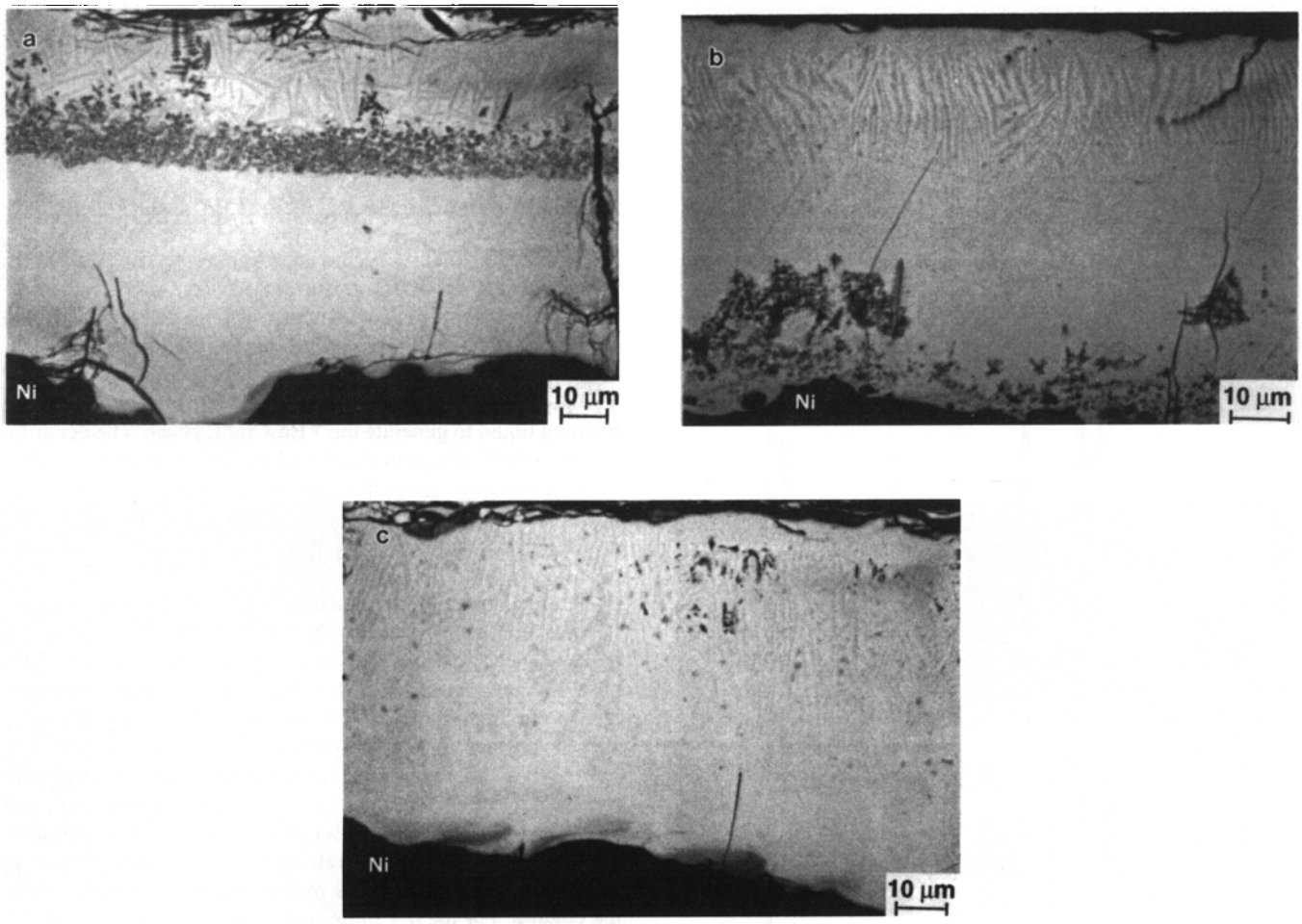

Fig. 5 Microstructure of laser-processed Y-base coatings using parameter No. 3 (0.5 J/mm) after (a) two passes, (b) three passes, and (c) seven passes.

sults. Minor constituents such as Y-123, $BaCO_3$, and Y_2BaCuO_5 (Y-211) are also present (Fig. 1c). These results indicate that flame melting of spray dried powder led to the formation of nonequilibrium phases during solidification. Moreover, the broad peak visible near 30° (2θ) suggests the presence of significant amounts of amorphous phase(s).

The Er-base powder fabricated in the laboratory is shown in Fig. 2. These angular particles were screened to sizes ranging between 10 and 64 μm. This powder essentially consisted of Er-123 with a few Er-211 inclusions and unreacted $BaCuO_2$ grains.

3.2 *As-Sprayed Coatings*

The two types of as-deposited coatings are shown in Fig. 3. In the Y-base coatings, particles were almost completely melted (Fig. 3a). Indeed, coatings were dense with thin lamellae, indicating a high velocity and temperature on impact. However, the Y_2O_3 (i.e., the dark phase in Fig. 3b) is not as uniformly dispersed in the as-sprayed coatings in spite of the high melting degree of the particles. Because the starting powder underwent an additional rapid solidification during plasma spraying, the same compounds are found in as-sprayed coatings,[15,16] i.e., major phases corresponding to Y_2O_3 and $BaCu_2O_2$ and minor phases corresponding to Y-123 and Y-211 phases. EDX analysis provided an overall composition close to $YBa_{1.8}Cu_{2.7}O_x$, indicating a significant loss of copper with respect to the Y-124 starting composition.

In the case of the Er-base coatings, selected spraying parameters led to a partial melting of the particles and, consequently, a porous coating (Fig. 3c). Partially melted $ErBa_2Cu_3O_x$ particles are visible in the cross section of the as-sprayed coating, and their presence is also confirmed by X-ray diffraction lines (Fig. 3d). In addition, nonequilibrium phases are also found: Er_2O_3 and $BaCu_2O_2$ along with minor phases corresponding to Er-211 and $BaCuO_2$ phases. It can be noted that no vaporization, as determined by excessive fuming, was observed during plasma spraying of this material.

3.3 *Laser Processing of Y-Base Plasma-Sprayed Coatings*

Figures 4(a) to (c) show the physical aspects of laser-treated Y-base coatings as a function of the laser processing parameter No. 1, 2, and 3, respectively (Table 2). These conditions represent a gradual decrease in the linear energy imparted to the specimen. The typical lamellae structure found in plasma-sprayed coatings disappeared after these laser treatments, and

Table 3 Average composition of coatings after successive laser scans using parameter No. 3 (see Table 2)

No. of passes	Elemental composition (atom fraction)			
	Y	Ba	Cu	Ni
1	0.20	0.32	0.48	0
3	0.27	0.40	0.31	0.02
7	0.46	0.40	0.10	0.04
15	0.92	0.05	0	0.03

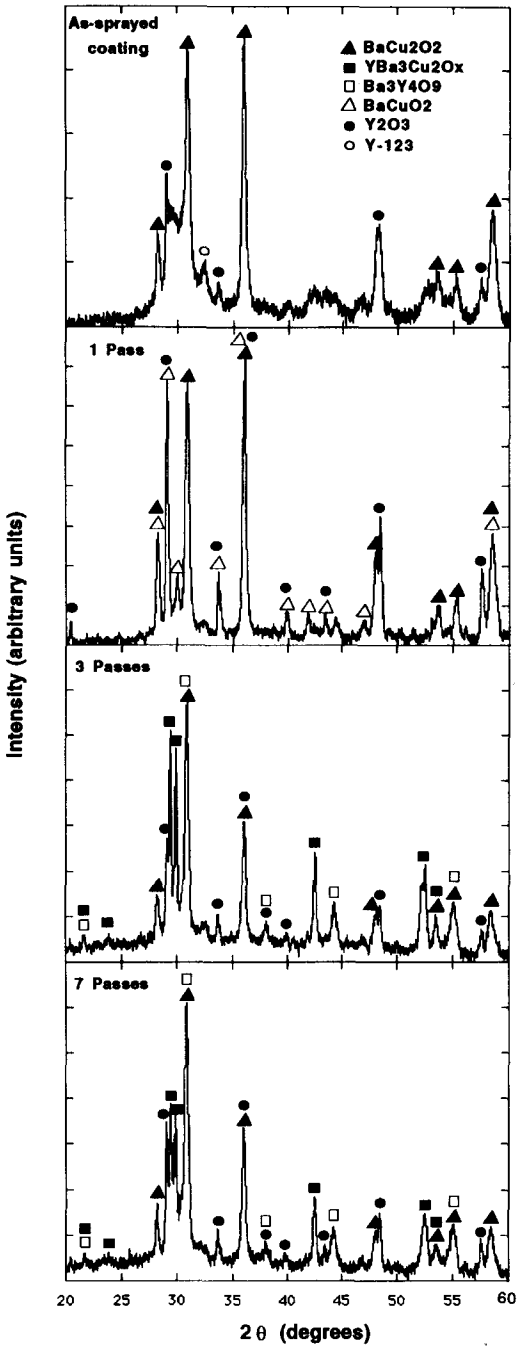

Fig. 6 XRD patterns of Y-base coatings as sprayed and after one, three, and seven laser passes using parameter No. 3 (0.5 J/mm).

densification occurred. The microstructures consist of a $BaCu_2O_2$ and $BaCuO_2$ matrix containing fine dendritic Y_2O_3 precipitates and many fine and large transversal (i.e., transverse with respect to the substrate surface) cracks. These nonequilibrium phases are due to the high cooling rates that prevail during solidification, impeding the completion of the two peritectic reactions, i.e., the reaction of Y_2O_3 with the liquid to yield Y_2BaCuO_5, which in turn should normally react with the remaining liquid to generate the $YBa_2Cu_3O_x$ phase. The dendritic nature of the Y_2O_3 precipitates and the featureless aspect of the remaining matrix suggest a very rapid solidification rate. The dendrites are primarily localized in the mid-layer of the coatings, probably corresponding to a slower cooling rate at the end of solidification.[15,16]

The morphology, size, and distribution of Y_2O_3 also provide insights into the thermal cycle during processing. Using the highest linear energy of 1 J/mm, cellular and dendritic Y_2O_3 phases were produced (Fig. 4a). This phase was primarily localized in the central portion of the coating and in a very thin layer near the surface. A large proportion of Y_2O_3 was considerably refined to a submicron size. Lower linear energy such as 0.85 J/mm led to cellular dendrites, with sizes ranging between 1 and 5 μm (Fig. 4b). With these laser processing conditions, the temperature at the coating/substrate interface was sufficiently high to melt the substrate because nickel globules were detected in the coating. For the 0.5 J/mm linear energy used in this series, fine Y_2O_3 dendrites formed and indicate that high cooling rates still prevailed at these conditions (Fig. 4c). It appears that this minimum linear energy of 0.5 J/mm was sufficient to completely melt these 200-μm thick coatings. This bimodal distribution of Y_2O_3 precipitates, as well as their heterogeneous dispersion, indicates that these laser processing conditions probably led to a transitory regime between a dendritic solidification mode and a crystallization of submicron second phases.

Laser processing the HTSC coatings with the three above-mentioned parameters produced microstructures that could be appropriate as precursors (or starting material) to produce the textured superconducting phase by melt/growth process. The size and distribution of phases in these coatings is similar to those used by Murakami:[13] fine Y_2O_3 precipitates dispersed in a Ba-Cu-O-rich matrix.

The effect of the number of passes was investigated for the latter laser processing conditions corresponding to the lowest linear energy used with the Y-base coatings. Figure 5 shows the microstructure of the coatings after two, three, and seven laser passes. The second pass (Fig. 5a) did not create a homogeneous microstructure, but produced a coarse dendritic microstructure in the upper half of the coating. This result could arise from an incomplete dissolution of the primary $BaCu_2O_2$ and Y_2O_3 and a local redistribution of these phases during the crystallization of the second pass. It could also be due to different heat penetration caused by modification of the thermal properties of the coating. Indeed, the first pass generated densification and a change in the

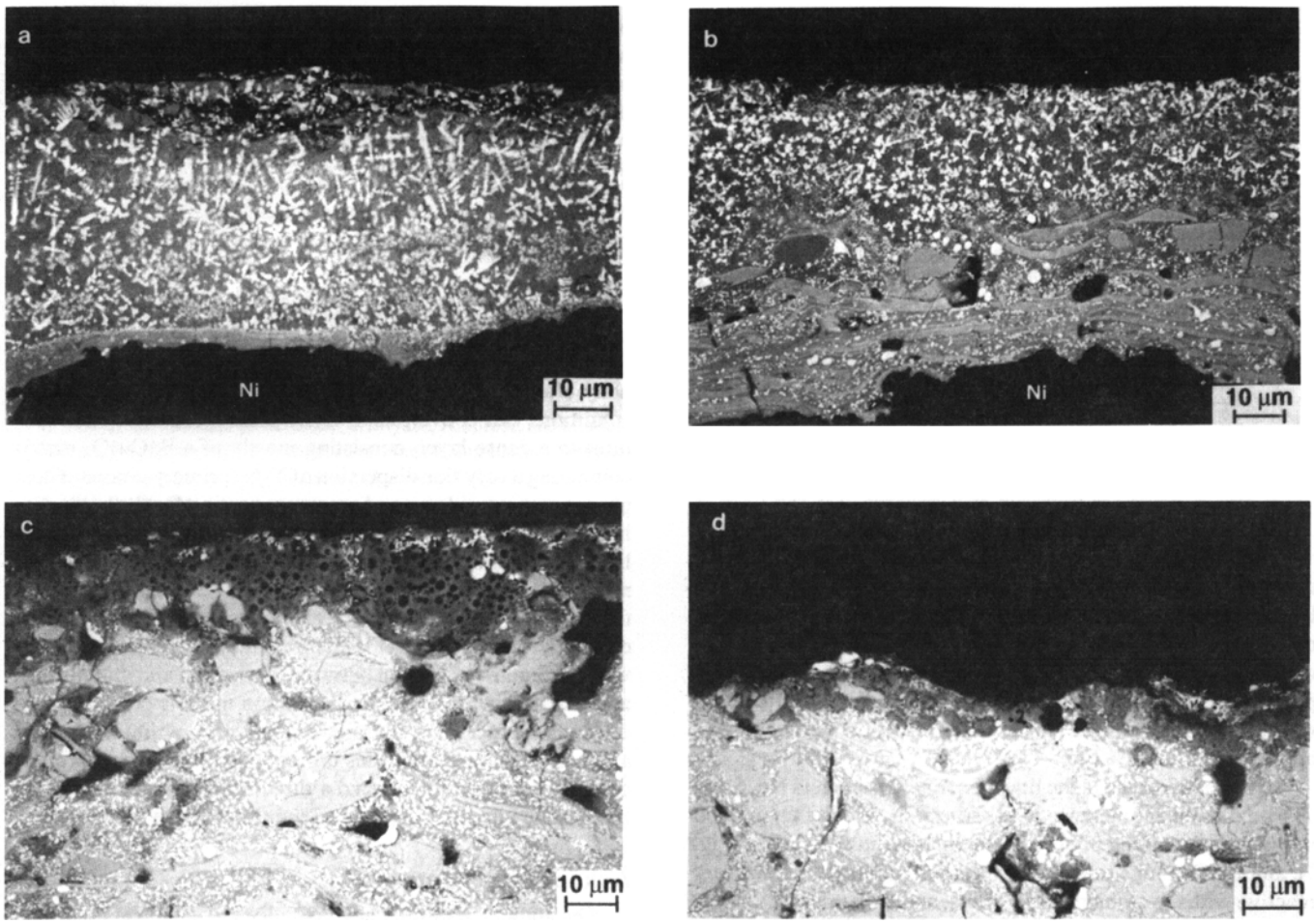

Fig. 7 Microstructure of laser-processed Er-base coatings using (a) 0.2 J/mm, (b) 0.1 J/mm, (c) 0.06 J/mm, and (d) 0.03 J/mm. These processing conditions are described as No. 4, 5, 6, and 7, respectively, in Table 2.

nature of phases. After three and seven passes (Fig. 5b and 5c), complete homogenization took place. However, chemical microanalysis of the coating (Table 3) reveals that the overall composition of coatings is strongly affected by the successive passes (1, 3, 7, and 15 passes). As the number of passes increased, a total loss of copper, an almost complete loss of barium, and an increase in the nickel contamination occurred. Such a modification of the cation stoichiometry largely altered the nature of phases crystallized in the coating and destroyed it. The XRD patterns (Fig. 6) show the evolution of phases in the coating after plasma spraying and after one, three, and seven laser passes using parameter No. 3. A small peak, attributed to the 123 phase, was observed after plasma spraying, but not after laser processing. After the first laser pass, only Y_2O_3 and Ba-Cu-O phases crystallized, whereas after three laser passes new phases (such as $Ba_3Y_4O_9$ and $YBa_3Cu_2O_x$,[17,18]) appeared. These phases still remain after seven passes. These results are different from the observations of Miyazawa et al.,[12] who reported the presence of 123 and $Ba_4Y_2O_7$ phases after four laser scans, but none of the $YBa_3Cu_2O_x$ phase. The phases present in the laser-treated coatings are very sensitive to the processing conditions and to the chemical composition of the coating. Therefore, reducing copper losses could produce a phase composition substantially different.

3.4 *Laser Processing of Er-Base Plasma-Sprayed Coatings*

For laser processing of Er-base coatings, a new series of parameters were selected to reduce the evaporation of barium and copper, the cracking, and the nickel contamination. The Er-base coating also allows a better phase contrast using the backscattered electron image mode of SEM over the Y-base coating material. The linear energy densities, E_L, used for laser processing these Er-base coatings were decreased by significantly increasing the laser scanning velocity. Furthermore, the lower incident energy input was partially compensated for by preheating the coatings at 800 °C during laser treatments.

Figure 7 shows the microstructure of Er-base coatings treated using parameters No. 4 to 7. As expected, the decrease in the incident linear energy, from parameters No. 4 to 7, reduced the thickness of the laser-melted layer. However, the thickness of the melted layer is nonuniform and seems to be affected by the presence of residual unmelted particles embedded in the coating

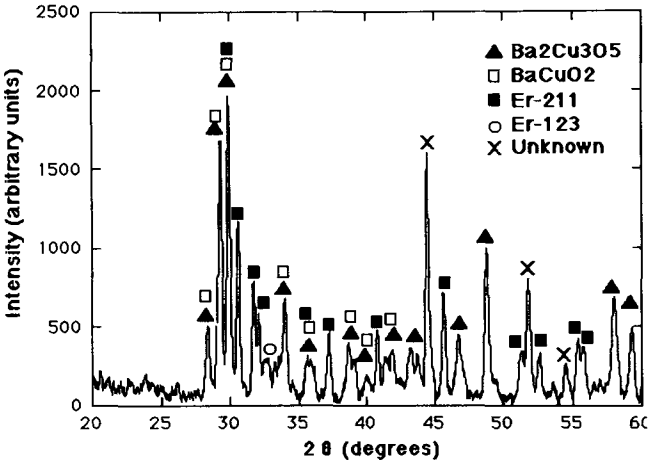

Fig. 8 XRD pattern of the top of the Er-base coating laser processed using parameter No. 6 (0.06 J/mm).

during plasma spraying. The cooling rate is locally influenced by this variation in the thickness of the melted layer. The shape of Er-211 and Er_2O_3 phases is dendritic in those coatings that completely melt (Fig. 7a, parameter No. 4) and rather rounded in partially melted coatings crystallized at higher solidification rates (Fig. 7b, parameter No. 5). The Ba-Cu-O matrix contains approximately 5 at.% Er.

A further decrease in the linear energy (parameters No. 6 and 7) by a significant increase in the scanning velocity up to 4000 mm/s caused melting of only a thin top layer in the coating (Fig. 7c and d). Coatings processed with such parameters were very reactive with the ambient atmosphere, and their microstructures were affected during polishing. The crystalline structure of this layer was probably also affected by reaction with ambient air. Figure 8 shows the XRD pattern of the coating processed using parameter No. 6. Because this coating was not completely melted during laser processing, the XRD pattern was not obtained with the ground coating, but rather by scanning the top surface of the coating, which could have induced a shift in the position of the peaks. The melted layer consists mainly of Er-211, $BaCuO_2$, and probably $Ba_2Cu_3O_5$ phases. This latter compound, which has an XRD pattern very similar to the $BaCuO_2$ phase, has already been observed in Ba-Cu-O samples heat treated at 940 °C.[18,19] Very little if any 123 phase was detected, and some peaks remained unidentified (Fig. 8). These results may be explained by the high reactivity of these laser-treated coatings.

Microanalysis of phases in the very unstable thin top layer of a coating laser treated using parameter No. 7 (Fig. 7d) yielded an atomic composition close to that of the 123 phase. No XRD analysis was carried out on this sample because of the thinness of the melted layer. This thin layer was quenched very rapidly upon laser processing, and it is possible that the solidification event by-passed the peritectic reaction. Indeed, the Er-123 phase may have nucleated directly from the liquid state, as suggested by Nagaya et al.[20]

As a general observation, it is important to mention that cracking was less severe in preheated Er-base coatings than in nonpreheated Y-base coatings, although a few small vertical cracks were still visible in the unmelted part of the Er-base coatings. As in the case of Y- base coatings, laser processing the Er-base coatings using the parameters listed in Table 2 produced microstructures that could be appropriated as precursors[18] to produce the superconducting phase. The formation of the superconducting phase may subsequently be achieved using other laser parameters[21] or techniques.[13,20-22]

4. Conclusions

Laser processing of as-sprayed HTSC coatings has been used to modify their microstructures. To obtain a homogeneous coating after laser processing, it is necessary to have good homogeneity after plasma spraying. A large range of laser processing conditions can convert as-sprayed Y-base coating microstructures to a dense layer, consisting mostly of a $BaCu_2O_2$ matrix containing a very fine dispersion of Y_2O_3 primary phases. Those phases may provide a good precursor coating for further texturing. However, the use of many successive laser passes at high linear energies brought about a loss of Cu and Ba, as well as significant coating/substrate interactions and extensive cracking of the coating. Under low linear energy conditions with Er-base coatings, microstructural transformations can be performed with minimum interaction between the coating and the substrate and practically no substrate dissolution into the coating. However, laser processing these coatings with low linear energies and high scanning velocities did not completely transform the coating, but possibly induced a direct transformation from the liquid state into the 123 phase as suggested in the literature.[13]

Acknowledgments

The authors gratefully acknowledge the technical assistance of B. Harvey and M. Thibodeau and wish to thank Dr. B. Marple and Mr. S. Turcotte for their critical review of the manuscript.

References

1. R.A.Neiser, J.P. Kirkland, W.T. Elam, H. Herman, S. Rangaswamy, V.M. Letourneau, and N. Osofsky, Electrical, Chemical and Structural Properties of Plasma-Sprayed Y-Ba-Cu-O Oxide Superconducting Coatings, *Mater. Res. Soc. Symp. Proc.*, Vol 99, 1988, p 689-693
2. J.J. Cuomo, C.R. Guarnieri, S.A. Shivashankar, R.A. Roy, D.S. Yee, and R. Rosenberg, Large Area Plasma Spray Deposited Superconducting $YBa_2Cu_3O_7$ Thick Films, *Adv. Ceram. Mater.*, Vol 2, 1987, p 422-429
3. G.N. Heintze, R. McPherson, D. Tolino, and C. Andrikidis, The Structure of Thermally Sprayed $YBa_2Cu_3O_{7-x}$ Superconducting Coatings, *J. Mater. Sci. Lett.*, Vol 7, 1988, p 251-253
4. L. Pawlowski, A. Gross, and R. McPherson, Microstructure of Plasma-Sprayed $YBa_2Cu_3O_7$ High-Temperature Superconductors, *J. Mater. Sci.*, Vol 26, 1991, p 3803-3808
5. D. Dubé, P. Lambert, B. Arsenault, and B. Champagne, Post-Deposition Treatments of Y-Ba-Cu-O Plasma Sprayed Coatings Deposited on Nickel, *Thin Solid Films*, Vol 193/194, 1990, p 847-856
6. S. Jin, R.C. Sherwood, T.H. Tiefel, R.B. van Dover, R.A. Fastnacht, and M.E. Davis, Processing for High Critical Currents in $YBa_2Cu_3O_7$, *High Temperature Superconductors II (Extended Abstracts)*, 1988 MRS Spring Meeting, Vol EA-14, 1988, p 153-156
7. M. Morita, M. Murakami, K. Miyamoto, K. Sawano, and S. Matsuda, Superconducting Properties of Bulk $YBa_2Cu_3O_{7-Y}$ Prepared by a Quench and Melt Growth Process, *Physica C*, Vol 162-164, 1989, p 1217-1218

8. K. Salama, V. Selvamanickam, L. Gao, and K. Sun, High Current Density in Bulk YBaCuO Superconductor, *Appl. Phys. Lett.*, Vol 54, 1989, p 2352-2354
9. P.J. McGinn, M.A. Black, and A. Valenzuela, Texture Processing of $YBa_2Cu_3O_{7-x}$ by Joule Heat Zone Melting, *Physica C*, Vol 156, 1988, p 57-61
10. J.R. Cave, P.R. Critchlow, P. Lambert, and B. Champagne, Calculation of Magnetic Flux Profiles and Deduction of Critical Current Densities for Type II Superconductors, *IEEE Trans. Magn.*, Vol 27, 1991, p 1379-1382
11. B. Arsenault, D. Dubé, and C. Gélinas, Laser Texturing: A Directional Solidification Technique to Reduce Material Transport During HTSC Texturing, *Proc. 2nd Int. Conf. Laser Advance Materials Processing—Science and Applications*, Vol 2, A. Matsunawa and S. Katayama, Ed., Nagaoka, Japan, 1992, p 849-854
12. H. Miyazawa, K. Hotta, S. Watanabe, S. Miyake, H. Hirose, and M. Murakawa, Preparation of Superconductive Films Using Plasma Sprayed Technique with Laser Post-Treatment, *Supercond. Sci. Technol.*, Vol 4, 1991, p 491-494
13. M. Murakami, The Quench and Melt Growth Process, *Supercurrents*, Vol 9, 1989, p 41-47
14. M.F. Yan, R.L. Barns, H. M. O'Bryan, Jr., P.K. Gallagher, R.C. Sherwood, and S. Jin, Water Interaction with the Superconducting $YBa_2Cu_3O_7$ Phase, *Appl. Phys. Lett.*, Vol 51 (No. 7), 1987, p 532-534
15. C.L. Teske and H. Muller-Buschbaum, Zur Kenntnis von $BaCu_2O_2$, *Z. Naturforch.*, Vol B27, 1972, p 296-301 in German
16. D. Dubé, B. Champagne, P. Lambert, and Y. LePage, Occurrence of $BaCu_2O_2$ in Plasma Sprayed YBaCuO Coatings, *Mater. Lett.*, Vol 9, 1990, p 353-356
17. J.-H. Shieh and S.-T. Wu, Rapid Solidification of a Plasma-Sprayed Ceramic Coating Melted by a CO_2 Laser, *Appl. Phys. Lett.*, Vol 59, 1991, p 1512-1514
18. P. Lambert, D. Dubé, C. Gélinas, and B. Arsenault, Effect of Precursors on the Size of 211 in Melt-Processed ErBaCuO, *Mater. Lett.*, in press
19. I. Halasz, V. Fulop, I. Kirschner, and T. Porjesz, Thermodynamical and X-Ray Diffraction Investigations of $Ba_2Cu_3O_{5+d}$ for Preparation of Y-Ba-Cu-O Superconductors, *J. Crystal Growth*, Vol 91, 1988, p 444-449
20. S. Nagaya, M. Miyajima, I. Hirabayashi, Y. Shiohara, and S. Tanaka, Rapid Solidification of High-Tc Oxide Superconductors by a Laser Zone Melting Method, *IEEE Trans. Magn.*, Vol 27, 1991, p 1487-1494
21. M.J. Cima, M.C. Flemings, A.M. Figueredo, M. Nakade, H. Ishii, H.D. Brody, and J.S. Haggerty, Semisolid Solidification of HTSC Oxides, *J. Appl Phys 72* (1), July, 1992
22. C. Gélinas, P. Lambert, D. Dubé, B. Arsenault, and J.R. Cave, Texturing of Thick Films on a Metallic Substrate, *Supercond. Sci. Technol.*, Vol 6, 1993, p 368-372